Journal of Power Sources 471 (2020) 228474

Contents lists available at ScienceDirect

Journal of Power Sources

journal homepage: www.elsevier.com/locate/jpowsour

Electrochemical cleaning: An *in-Situ* method to reverse chromium poisoning in solid oxide fuel cell cathodes

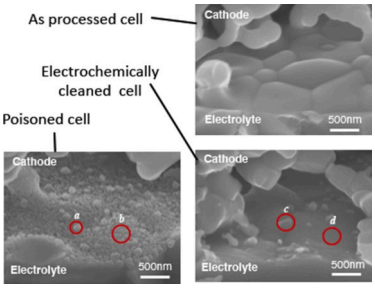
Zhikuan Zhu [a], Michelle Sugimoto [b], Uday Pal [a,b], Srikanth Gopalan [a,b], Soumendra Basu [a,b,*]

[a] Department of Mechanical Engineering, Boston University, Boston, MA, 02215, USA
[b] Division of Materials Science and Engineering, Boston University, Brookline, MA, 02446, USA

HIGHLIGHTS

- Chromium poisoning leads to formation Cr_2O_3 and (Cr,Mn) spinel deposits.
- Chromium poisoning leads to significant degradation in cell performance.
- An *in-situ* electrochemical cleaning process can reverse chromium poisoning.
- The electrochemical cleaning process removes all the Cr_2O_3 deposits.
- The cell exhibits significant restoration of performance after electrochemical cleaning.

GRAPHICAL ABSTRACT



ARTICLE INFO

Keywords:
Solid oxide fuel cell
Chromium poisoning
Cathode degradation
Solid oxide electrolyser cell
Electrochemical cleaning
Performance recovery

ABSTRACT

Chromium poisoning is one of the primary factors that affect solid oxide fuel cell (SOFC) durability. In this study, an electrochemical cleaning method has been employed to reverse the effects of chromium poisoning. Two cells were fabricated and poisoned under identical conditions by operating them at 800 °C in the presence of a Cr source. Both poisoned cells exhibited a significant reduction in maximum power density and an increase in polarization resistance. One of the poisoned cells, designated as the baseline cell, was cooled to room temperature after poisoning. Microstructural observation of the baseline cell showed significant contamination of the cathode active layer by chromium oxide and (Cr,Mn) spinel deposits. The other poisoned cell was electrochemically cleaned for 2 h under a mild electrolytic condition. As a result of the electrochemical cleaning process, the chromium oxide deposits were substantially removed leading to a significant reduction of Cr concentration in the cathode, especially at the cathode/electrolyte interface. A substantial fraction of the cell performance loss was also reversed. To the best of our knowledge, this is a first demonstration of reversing the effects of chromium poisoning using a rapid *in-situ* process.

1. Introduction

Solid oxide fuel cells (SOFCs) have several advantages as electrochemical energy generation devices, including high energy conversion efficiency, negligible emissions, and high fuel flexibility [1,2]. SOFCs have been used in a variety of applications, including distributed power generation, electric vehicles, and portable power devices [3–6]. However, durability issues still limit the commercial viability of SOFCs. At

* Corresponding author. Department of Mechanical Engineering, Boston University, Boston, MA, 02215, USA.
E-mail address: basu@bu.edu (S. Basu).

https://doi.org/10.1016/j.jpowsour.2020.228474
Received 30 March 2020; Received in revised form 4 June 2020; Accepted 8 June 2020
Available online 28 June 2020
0378-7753/© 2020 Elsevier B.V. All rights reserved.

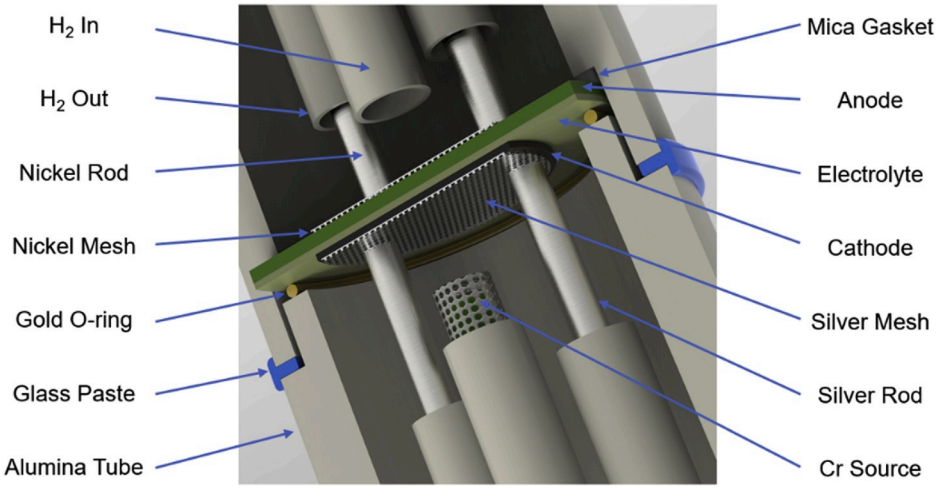


Fig. 1. Schematic of cell test setup.

high temperature operating conditions, volatile hexavalent chromium oxide/hydroxide species are formed from the thermally grown oxide scale on stainless steel interconnects and balance of plant components. These vapor phase species are reduced and deposited on the electrochemically active areas in the cathode. This phenomenon, known as 'chromium poisoning,' is one of the primary reasons for long-term degradation of SOFC performance [7–10].

Despite substantial research on chromium poisoning, there is still significant disagreement on the nature of Cr-containing deposits and their effects on cell performance. The general consensus is that at high temperatures, thermally grown Cr_2O_3 scales are formed at the surface of the stainless-steel interconnects and balance of plant (BOP) components. Then, Cr-containing vapor species such as CrO_3(g), $CrO_2(OH)_2$(g), and CrO_2OH(g) are generated under airflow, with the hydroxide-containing species forming in the presence of water vapor. Increasing the air humidity and temperature increases the partial pressure of the Cr-containing vapor species [11,12]. Such Cr species are then reduced, deposit in the porous cathode under current load, and impede the oxygen reduction reaction (ORR). Different Cr-containing deposits have been found depending on the cathode material. For strontium-doped lanthanum manganite (LSM) or LSM/yttria-stabilized zirconia (YSZ) based cathodes, the primary deposits have been reported to be Cr_2O_3 and (Cr,Mn) spinel [7,13,14]. For lanthanum strontium cobalt ferrite (LSCF) or lanthanum strontium ferrite (LSF) based cathode, the primary deposits have been reported to be Cr_2O_3 and $SrCrO_4$ [15].

Many solutions have been proposed to mitigate chromium poisoning, including using more Cr-tolerant cathode materials [16], gettering of the Cr-containing vapor species before they reach the cathode [13], applying diffusion resistant coatings on interconnects [17,18], and using alumina forming alloys for BOP components [19–21]. In all of these cases, substantial and expensive changes have to be made to existing SOFC systems. Many of these techniques impede chromium poisoning for a period of time, but are not able to ensure reliable SOFC performance over the lifetime of the device.

In this study, we demonstrate the feasibility of a novel method we have termed 'electrochemical cleaning.' The *in-situ* process, based on the reversible operation of LSM-based cells, removes the chromium deposits from the cathode. Previous studies have shown that the mechanism of Cr poisoning is electrochemical in nature [7,22–25]. The overall cell reaction equations for Cr deposition involving CrO_3(g), the most abundant Cr-containing vapor species in dry air, and $CrO_2(OH)_2$(g) and CrO_2OH(g), most abundant in humidified air, are shown below.

$$2CrO_3(g, \text{air side}) + 3H_2(g, \text{fuel side}) = Cr_2O_3(s, \text{air side}) + 3H_2O(g, \text{fuel side}) \quad (1)$$

$$2CrO_2(OH)_2(g, \text{air side}) + 3H_2(g, \text{fuel side}) = Cr_2O_3(s, \text{air side}) + 2H_2O(g, \text{air side}) + 3H_2O(g, \text{fuel side}) \quad (2)$$

$$3CrO_2(OH)\ (g, \text{air side}) + 3H_2(g, \text{fuel side}) = 3/2Cr_2O_3(s, \text{air side}) + 3/2H_2O\ (g, \text{air side}) + 3H_2O(g, \text{fuel side}) \quad (3)$$

Equations (1)–(3) require the transport of oxygen ions across the electrolyte from the air side to the fuel side. In the electrochemical cleaning method, the Cr deposition reactions are reversed by operating the device in reverse, i.e., as a solid oxide electrolyser cell (SOEC). During the application of an electrolytic current, oxygen ions are transported across the electrolyte to the air side from the fuel side, converting the deposited Cr_2O_3 into Cr-containing vapors species. This reaction is enhanced by increasing the temperature and the humidity on the air side.

In this study, two cells were fabricated and tested; a poisoning baseline and a cell that was poisoned and then electrochemically cleaned. To demonstrate the effect of cleaning, both cells were exposed to Cr vapor species under identical SOFC working conditions, leading to degradation of cell performance. Electrochemical cleaning was then applied to one cell under SOEC conditions. Current-voltage (I–V) and electrochemical impedance spectroscopy (EIS) data were acquired were to evaluate cell performance. Microstructural characterization of poisoned and electrochemically cleaned cells was carried out using scanning electron microscopy (SEM) and energy dispersive x-ray spectroscopy (EDS). The results showed that after electrochemical cleaning, most of the Cr-containing deposits were removed compared to the poisoning baseline cell. This was accompanied by a significant recovery of cell performance as a result of cleaning.

2. Experimental methods

In this work, button half cells were commercially purchased from SOFCMAN Energy (Ningbo, China). The half cells consisted of a 400 μm thick NiO-8YSZ (8 mol% Y_2O_3-92 mol% ZrO_2) anode substrate, a 7 μm thick NiO-8YSZ anode active layer, and a 7 μm thick dense YSZ electrolyte. Cathode slurries were prepared before screen printing by mixing the desired cathode powders and then ball milling with alpha-terpineol (Alfa Aesar), carbon black pore former (Fisher Scientific), and binder (V6, Heraeus). A 1:1 wt ratio of $(La_{0.8}Sr_{0.2})_{0.9}MnO_{3-\delta}$ (Fuel Cell Material) and 8YSZ (Tosoh Corp) powders was used for the cathode active layer. Only LSM powder was used for the cathode current collector layer. The two layers, each 25 μm thick, were screen printed on the electrolyte and sintered separately at 1200 °C for 2 h [25,26]. The diameters of the NiO-YSZ substrate and cathode were 3 cm and 1.6 cm, respectively.

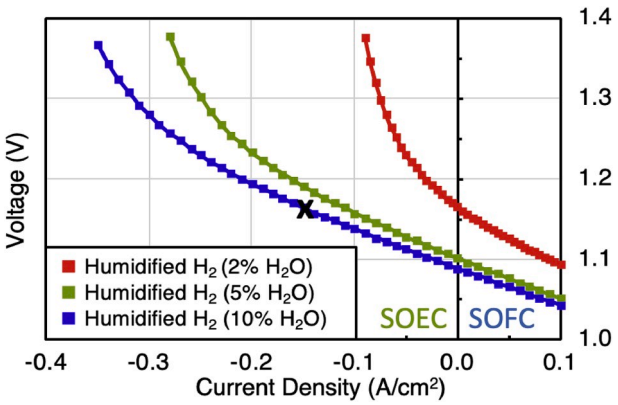


Fig. 2. I–V curves for a Cr-free cell operated at 800 °C under varying fuel humidity values at the fuel electrode and dry air at the air electrode. Positive current corresponds to the SOFC mode and negative current to electrolytic mode. The electrochemical cleaning condition used in this study is designated by X.

The fabricated cathodes were purposely designed with large grain sizes and high porosity to reduce the triple phase boundary (TPB) length. With this specific microstructure, less deposited chromium is needed to have a large effect on cell performance as evidenced by I–V and EIS analyses. Thus, the changes in performance are enhanced in this study to elucidate performance changes with changes in the concentration of Cr-containing deposits within the cathode.

Before loading the cell into the test stand (Fig. 1), a silver mesh (Fuel Cell Materials) was attached using Ag paste on the air side of the cell, and nickel mesh (Alfa Aesar) was attached using Ni paste on the fuel side. Both served as current collectors. The cell was sandwiched between two alumina tubes, with a gold O-ring and mica gasket (Fuel Cell Materials) used as seals on either side. The outside of the tube was sealed with glass paste (Fuel Cell Store). Spring-loaded silver wire and nickel rods (Alfa Aesar) were used for electrical conduction. Small Cr_2O_3 pellets (Alfa Aesar) were wrapped inside a silver mesh (Alfa Aesar) and attached to the end of a retractable ceramic tube, which supplied humidified air during poisoning [27]. During the poisoning phase, the Cr_2O_3 bundle was positioned ~1 cm from the air electrode in the hot zone to facilitate Cr vaporization.

All cell testing was conducted at 800 °C. For cell stabilization, a fuel gas mixture of 98% H_2 – 2% H_2O was supplied to the cell at a flow rate of 300 cm^3/min by bubbling pure hydrogen through a water bath at room temperature, establishing a low fuel utilization condition. Dry air was supplied at 1000 cm^3/min by passing compressed air through a desiccant, which also established a low oxygen utilization condition. Both cells were first stabilized for 48 h using 0.5 A/cm^2 applied current density.

During the Cr-poisoning phase, the air humidity was increased to 5% to increase the rate of Cr vaporization and thus deposition onto the cathode. This was accomplished by bubbling air through a water bath maintained at 33 °C. The Cr source was introduced into the air flow. The cells were exposed to Cr vapors for 120 h under 0.5 A/cm^2 current density. The Cr source was then removed from the air flow. The poisoning baseline cell was cooled down at this point.

The other poisoned cell was electrochemically cleaned for 2 h under a mild electrolytic current of 0.15 A/cm^2. 10% humidified air on the air side and 10% humidified H_2 on the fuel side were supplied to the cell by passing each gas stream through their respective water baths maintained at 46 °C. The fuel humidity was chosen to allow for a higher electrolytic current without polarizing the cell. High electrolytic cell polarization conditions can result in cell degradation causing void formation in YSZ grain boundaries and delamination of the air electrode [28]. Fig. 2 demonstrates the significant impact low fuel humidity has on cell polarization in the SOEC mode, i.e. negative current regime. Hydrogen with 10% water vapor was chosen to limit cell polarization in the SOEC mode. Based on Fig. 2, the electrochemical cleaning condition was chosen to be 10% fuel humidity with an electrolytic current density of 0.15 A/cm^2 (marked by X in Fig. 2). This limited the overpotential to 0.075 V for a Cr-free cell. Chromium deposition causes an increase in the various polarizations across the cell. Therefore, the measured voltage under these conditions of a poisoned cell, i.e., during the cleaning phase in this study, is higher. The overpotential of the poisoned cell starts at 0.18V, and drops to 0.09V after electrochemical cleaning. However, as is discussed below, cell degradation as a result of operating the cell in SOEC mode was not observed under the conditions used in this study.

Current-voltage (I–V) and electrochemical impedance spectroscopy (EIS) measurements were acquired between each test phase to quantify changes in cell performance. All measurements were acquired at 800 °C, under dry air (air side) and 2% humidified hydrogen (fuel side). Adequate time (~1 h) was given before each I–V and EIS measurement to ensure cell equilibration. Electrochemical measurements were conducted using a Princeton Applied Research 263A PARSTAT®, KEPCO COP 20-20 M power amplifier, and a Solartron SI 1250 frequency response analyzer.

Fractured samples were examined under the SEM to observe the microstructure of Cr-containing deposits after poisoning and after electrochemical cleaning. Samples were also mounted in cross-section in epoxy and polished for quantitative analysis of the Cr concentration profile across the cathode. After sputter coating both types of samples with carbon, samples were examined using scanning electron microscopy (Zeiss Supra 55 VP) and energy dispersive spectroscopy (EDS, Oxford Instruments, High Wycombe, UK). The acquired EDS spectra were analyzed using AZtec software (Oxford Instruments, High Wycombe, UK).

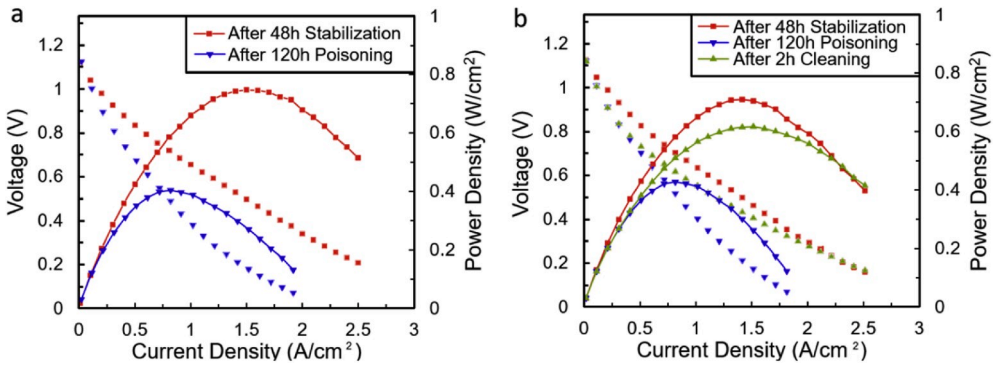


Fig. 3. Current voltage curves for the (a) poisoned baseline cell, and the (b) electrochemically cleaned cell. Measurements were obtained at 800 °C under dry air (air side) and 2% humidified H_2 (fuel side).

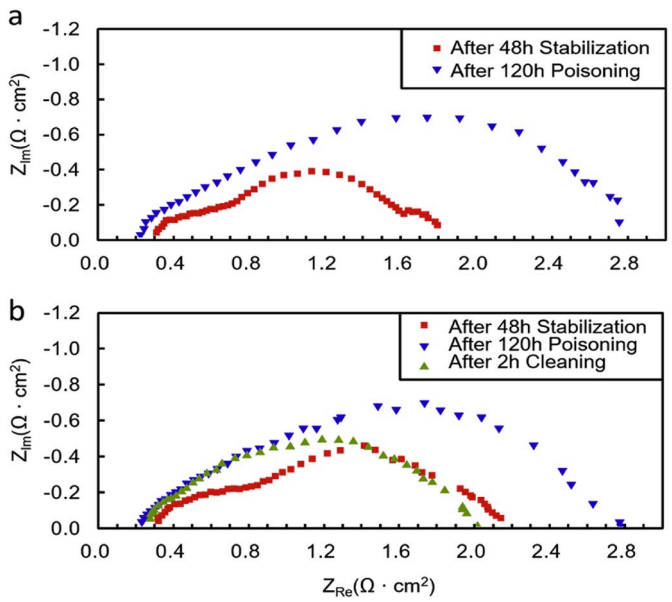


Fig. 4. EIS curves for the (a) poisoned baseline cell and (b) electrochemically cleaned cell. Measurements were taken at 800 °C under dry air (air side) and 2% humidified H_2 (fuel side) under open circuit condition.

3. Results and discussion

Fig. 3a shows the changes in performance for the poisoning baseline cell. After stabilization, the maximum power density, used as an indicator of cell performance, was 0.753 W/cm^2. This dropped down to 0.403 W/cm^2 after 120 h of Cr-poisoning, which constitutes a 46% drop in performance. Similarly, the cell that was electrochemically cleaned, started at a power density of 0.712 W/cm^2 after stabilization and dropped down to 0.428 W/cm^2, which is a 40% drop in performance (Fig. 3b). After electrochemical cleaning, the maximum power density increased to 0.617 W/cm^2. Compared to the stabilized cell before poisoning, application of these specific electrochemical cleaning conditions for 2 h resulted in a 67% recovery in cell performance.

Previous studies have shown that Cr-containing deposits form at the triple phase boundaries between the pore (gas phase), YSZ, and LSM phases near the cathode/electrolyte interface. The Cr-rich deposits block the electrochemically active sites, increasing the cathodic activation polarization. Also, the solid Cr-containing deposits reduce pore volume, increasing cathodic concentration polarization [29]. Both mechanisms lower cell performance. The recovery in the I–V curve as a result of cleaning demonstrates the removal of Cr-containing deposits from the TPBs, reversing the two deleterious mechanisms of chromium poisoning.

Fig. 4a and b shows the impedance spectra for the two cells measured under open-circuit condition. The high frequency intercept on the real (x) axis provides the ohmic resistance (R_Ω) of the cell, interconnects, and lead wires, while the low frequency intercept corresponds to the total resistance including the ohmic resistance as well as the polarization resistance (R_P). Thus, R_P is the difference between the two intercepts and includes the activation and concentration polarization resistances of the cell.

The ohmic resistance of the cell decreases slightly over the course of cell operation, which is expected. It has been observed by several researchers that the ohmic resistance of the cell can continue to decrease for many hours during SOFC operation even in the presence of a chromium source [30,31]. This trend has been attributed to improved contact resistance between the various cell components. The changes in polarization resistance however mirror the changes observed in the maximum power density. For both cells, R_P increased after poisoning, and for the cell that was electrochemically cleaned, R_P decreased after cleaning. The increase in R_P is commonly observed as a result of poisoning and results from Cr deposits blocking electrochemically active sites and thus hindering the oxygen reduction reaction [22,25,29,31]. Therefore, the subsequent decrease in R_P as a result of cleaning demonstrates the reversal of performance degradation by freeing the electrochemically active sites. Both I–V and EIS results corroborate the improvement in cell performance due to electrochemical cleaning of the poisoned cell.

SEM-based EDS analyses were conducted on the two cells after electrochemical testing to determine the amount of Cr-containing

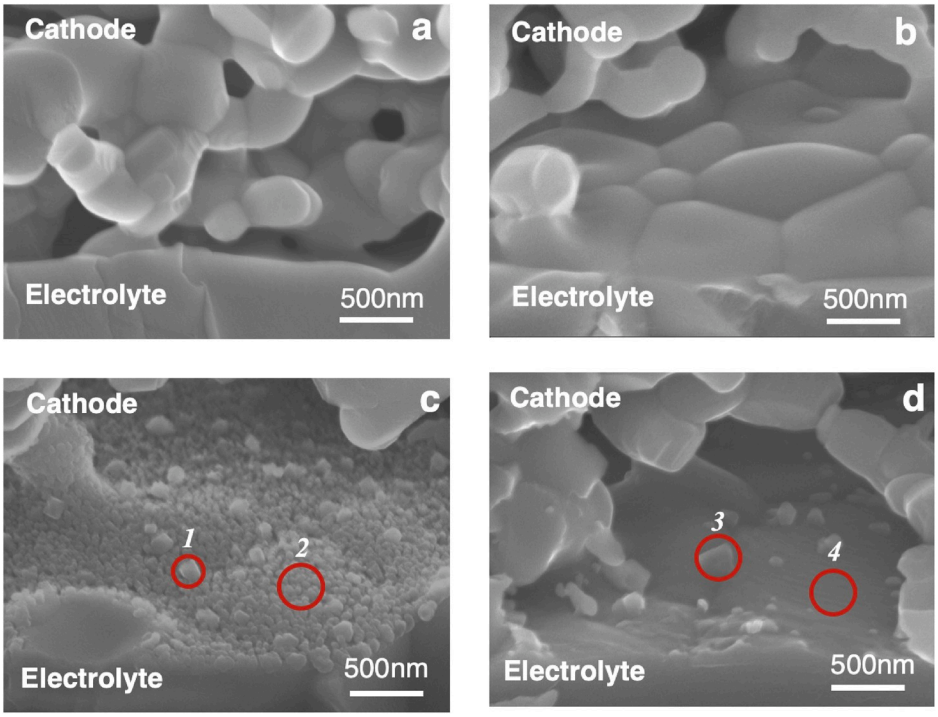


Fig. 5. SEM micrograph of cathode/electrolyte interface for an untested cell with the sample holder a) with no tilt and b) tilted at 30°. The interface is clean with no deposits observed. SEM micrograph of the electrolyte surface in the (c) poisoned baseline cell, with large and small deposits visible in regions marked as 1 and 2. SEM micrograph of the electrolyte surface in the (d) electrochemically cleaned cell, showing that the larger faceted deposits remain (region marked as 3) and the finer deposits are no longer present (region marked as 4). For micrographs (c) and (d), the sample holder is tilted at 30°.

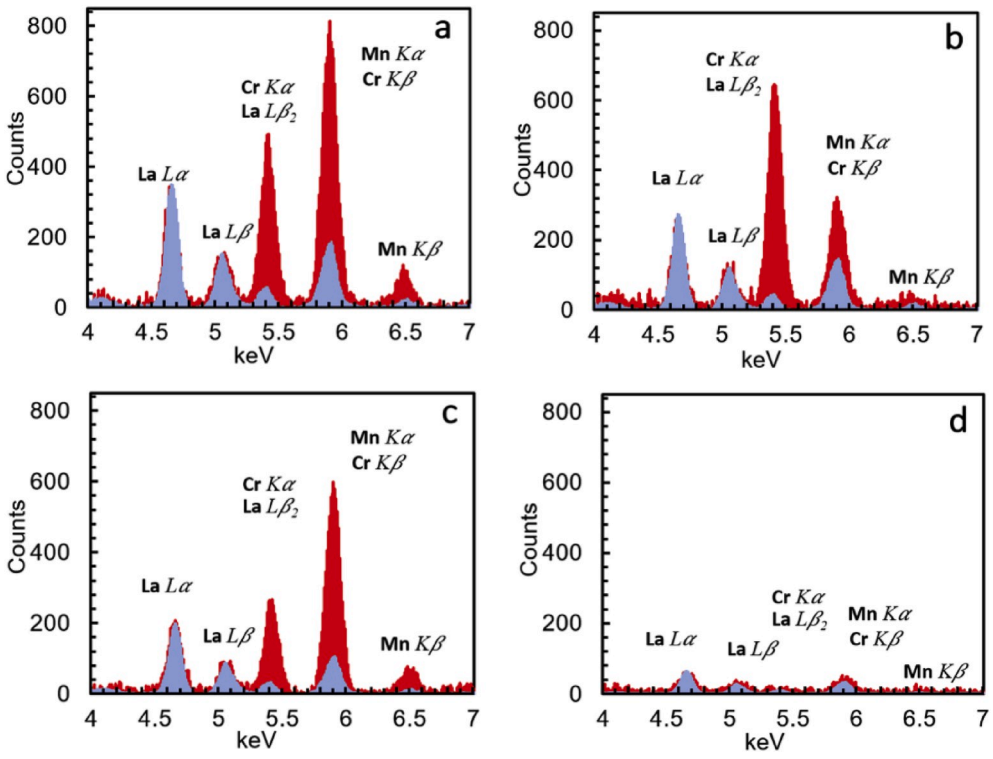


Fig. 6. The red EDS spectra are taken from (a) a large, faceted deposit (Region 1 in Fig. 5c) and from (b) a region with many fine, rounded deposits (Region 2 in Fig. 5c) in the poisoned baseline cell. The red EDS spectra are taken from (c) a large, faceted deposit (Region 3 in Fig. 5d) and from (d) a region without deposits (Region 4 in Fig. 5d) on the electrolyte surface in the electrochemically cleaned cell. All spectra are scaled to the blue reference spectrum for pure LSM. (For interpretation of the references to colour in this figure legend, the reader is referred to the Web version of this article.)

deposits present in each cell and to determine the nature of the Cr-containing deposits. Fig. 5a and b shows SEM micrographs of an untested cell. Here, the YSZ electrolyte surface and LSM/YSZ grains in the cathode are clean and devoid of any deposits. In comparison, the poisoned baseline cell, shown in Fig. 6c, show that the electrolyte surface at the electrolyte/cathode interface was covered with many small, rounded deposits as well as larger, faceted deposits. The larger deposits (see region marked as 1 in Fig. 5c) ranged from 100 to 200 nm in size, while the smaller deposits (see region marked as 2 in Fig. 5c) ranged from 20 to 50 nm in size.

EDS spectra from Region 1 (large faceted deposit) and 2 (small rounded deposits) of the poisoned baseline cell (Fig. 5c) are shown in red in Fig. 6a and b, respectively. We cannot directly compare the measured intensities of either Cr peak (at ~5.4 keV and ~5.9 keV) since the background LSM grains contribute to the 5.4 keV peak as La$L\beta_2$ and to the 5.9 keV peak as Mn$K\alpha$. Instead, the ratios between peaks can be used to compare Cr as well as Mn content in the deposits [32–34]. Since the La$L\alpha$ peak in the spectra (at ~4.65 keV) can only come from nearby LSM grains in the cathode, an EDS spectrum from an LSM grain in the clean untested cell can be used as a reference. The reference LSM spectrum is shown in blue in all four plots in Fig. 6. All spectra from the deposits are scaled with the reference spectrum such that the La$L\alpha$ peak intensity of the deposit spectrum is the same as that from the LSM reference spectrum. The ratio of La$L\beta_2$/La$L\alpha$ peak intensities is fixed for pure LSM. Thus, the relative intensity ratio, (Cr$K\alpha$ +La$L\beta_2$)/La$L\alpha$, can be used as an indicator for Cr concentration, and the ratio, Mn$K\beta$/La$L\alpha$ can be used as an indicator for Mn concentration, in the deposits. In other words, in the scaled deposit spectra (shown in red), elevation of the peak at ~5.4 keV relative to the peak at ~ 4.65 keV is indicative of the presence of Cr in the deposits. An increase in the intensity of the peak at ~6.5 keV relative to the peak at ~4.65 keV is indicative of the presence of Mn in the deposits.

The EDS spectrum (Fig. 6a) from the larger, faceted deposits (Region 1 in Fig. 5c) shows a relative elevation of both peaks (at ~ 5.4 keV and ~6.5 keV), indicating that the faceted deposit is rich in Cr and Mn. Thus, the larger, faceted deposits have been identified as (Cr,Mn) spinel. The EDS spectra (Fig. 6b) from the finer, rounded deposits (Region 2 in Fig. 5c) shows a relative elevation of only the peak at ~5.4 keV, indicating that the rounded deposits are only rich in Cr. Thus, these finer, rounded deposits have been identified as Cr_2O_3. The observation of the two deposit types and their identification by composition as well as general morphology has been reported in many previous studies [7,13,14].

The effect of electrochemical cleaning is clear when comparing the SEM micrographs of the poisoned baseline and the electrochemically cleaned cells (Fig. 5c and d). Fig. 5d shows that a majority of the deposits were removed from the electrolyte surface as a result of electrochemical cleaning. The EDS spectrum from a clean region (Region 4 in Fig. 5d) is shown in Fig. 6d. The spectrum shows there is no Cr or Mn enhancement, indicating that the deposits were completely removed from these regions by electrochemical cleaning. The SEM micrograph of the electrochemically cleaned cell (Fig. 5d) also shows that the large, faceted deposits still remain on the electrolyte surface (Region 3). Fig. 6c shows an EDS spectrum from the large faceted deposit in Region 3, showing the faceted deposit to be (Cr,Mn) spinel. Although four representative EDS spot analyses, two each for poisoned and cleaned samples are reported in the paper, around forty areas were analyzed, twenty for each sample. All of the spot scans were consistent with the fact that rounded deposits were Cr_2O_3, and faceted deposits were (Cr,Mn) spinels, and that after cleaning the Cr_2O_3 deposits were removed and the remaining deposits were (Cr,Mn) spinels. Furthermore, SEM images demonstrate that the mild electrolytic bias applied was sufficient to remove Cr deposits, while avoiding delamination between the electrolyte and air electrode, a common failure mechanism for SOECs.

The electrochemical cleaning process almost completely removes the Cr_2O_3 deposits, but leave the (Cr,Mn) spinel deposits behind. This can be partially explained by the difference in vaporization kinetics between the two deposit types. The Cr vapor species are more readily produced over pure Cr_2O_3 compared to (Cr,Mn) spinel. During transpiration tests conducted at 800 °C under 2% humidified air, Stanislowski et al. found that chromium vaporized from $(Mn,Cr)_3O_4$ at 30% of the rate of vaporization from Cr_2O_3 [21]. Chromium removal from (Cr,Mn) spinel

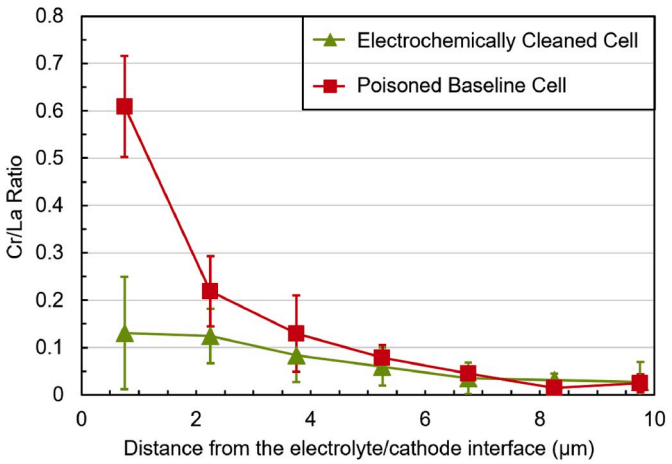


Fig. 7. Plot of Cr/La (atomic%) ratio, quantified using EDS measurements, as a function of the distance from the electrolyte into the cathode.

deposits is thus expected to be limited by the diffusion of Cr to the surface of the spinel deposit. Furthermore, chromium poisoning studies by Jiang et al. found that the formation of (Cr,Mn) spinel is due to its stability in SOFC operating conditions and is not electrochemical in nature [16].

The Cr concentration profile was measured by EDS on polished cross-sections of the poisoned baseline and the electrochemically cleaned cells. Fig. 7 shows the change in the Cr concentration (normalized to La) across the cathode thickness after poisoning (baseline) and after electrochemical cleaning. The (atomic %) ratio of Cr/La was determined at various depths in the cathode. Each value was averaged over 5 spectra, each obtained from rectangular areas, 1.5 μm thick and 40 μm long, all at a given distance from the electrolyte/cathode interface. Fig. 7 demonstrates a significant difference in the Cr concentration profiles between the two cells. Both cells demonstrate a higher Cr concentration closer to the electrolyte as expected for LSM/YSZ cathodes in the presence of chromium under cathodic polarization. However, the electrochemically cleaned cell demonstrates a significant decrease in the total amount of chromium compared to the poisoned baseline cell. At the cathode/electrolyte interface, where the Cr concentration is highest, the difference in Cr content between the poisoned baseline cell and the electrochemically cleaned cell is ~78%. Thus, under the conditions used, the electrochemical cleaning method is most effective on Cr_2O_3 deposits, which constitute the majority of the Cr deposition as qualitatively evidenced by Fig. 5c, and quantitively by the decrease in total Cr concentration (Fig. 7).

The poisoning and cleaning mechanisms are shown schematically in Fig. 8a and 8 b, respectively. Previous studies have shown that Cr deposition from the vapor phase in the air electrode occurs under cathodic conditions, i.e., when the cell operates as an SOFC. These deposits are not seen under OCV conditions [25,27]. This indicates that the Cr deposition reaction is electrochemical in nature. By operating the cell in the electrolytic mode, i.e., as a SOEC we observed the removal of the Cr oxide deposits and so we hypothesize that the removal mechanism must also be electrochemical and occurs by reforming chromium-containing vapor species that leave the system with the air flow.

Future studies will focus on optimizing the cleaning parameters, examining multiple poisoning/cleaning cycles, and a more detailed examination of the cleaning mechanism. More aggressive electrolytic cleaning conditions may remove the (Cr,Mn) spinel deposits, but may also damage the cell. These issues will be explored for LSM based cells, as well as for cells with different cathode materials.

4. Conclusions

In this study, LSM based solid oxide fuel cells were fabricated and tested at 800 °C. After poisoning with humidified air passing through Cr_2O_3, under cathodic current, performance degradation due to Cr-poisoning was observed. SEM and EDS analyses of the poisoned baseline cell revealed two types of Cr deposits: Cr_2O_3 and (Cr,Mn) spinel. The Cr_2O_3 deposits covered the entire YSZ electrolyte surface and extended several micrometers into the cathode. These deposits inhibited the ORR reaction and led to performance degradation of the cell in terms of a decrease in maximum power density and an increase in polarization resistance.

Electrochemical cleaning was implemented by operating the cell in the SOEC mode. A mild electrolytic cleaning condition was chosen to avoid irreversible damage to the cell. I–V and EIS analyses corroborated that chromium poisoning was reversed via electrochemical cleaning. Moreover, the electrochemically cleaned cell shows a relatively clean cathode/electrolyte interface, indicating that most of the Cr_2O_3 deposits were removed. This was accompanied by a significant recovery of the cell performance, i.e., an increase in the maximum power density and a reduction in the polarization resistance. Some deposits remained after cleaning and were identified to be (Cr,Mn) spinel, which are difficult to remove by the electrochemical cleaning conditions used in this study. This research demonstrates, for the first time, the reversal of the chromium poisoning using an *in-situ* electrochemical cleaning process. It is anticipated that fuel cell stacks can be periodically run in electrolytic mode for 2 h to substantially reverse the deleterious effects of chromium poisoning without having to cool the system down to room temperature.

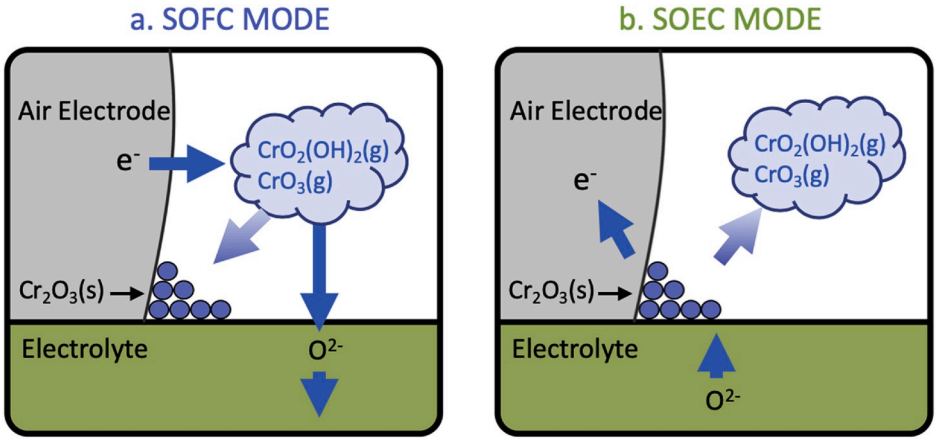


Fig. 8. Mechanisms for (a) chromium poisoning and (b) electrochemical cleaning of Cr deposits at a triple phase boundary, which occur in fuel cell (SOFC) mode and electrolyser (SOEC) mode, respectively.

Declaration of competing interest

The authors declare that they have no known competing financial interests or personal relationships that could have appeared to influence the work reported in this paper.

CRediT authorship contribution statement

Zhikuan Zhu: Investigation, Validation, Formal analysis, Data curation, Writing - original draft, Resources, Visualization. **Michelle Sugimoto:** Investigation, Validation, Data curation, Formal analysis, Writing - original draft, Resources. **Uday Pal:** Writing - review & editing, Supervision, Project administration, Funding acquisition. **Srikanth Gopalan:** Writing - review & editing, Funding acquisition. **Soumendra Basu:** Writing - review & editing, Supervision, Project administration, Funding acquisition.

Acknowledgements

This work was supported, in part, by the U. S. Department of Energy, Office of Fossil Energy, under Award Number DE-FOA-0001735.

References

[1] B.C.H. Steele, Running on natural gas, Nature 400 (6745) (1999) 619–621, https://doi.org/10.1038/23144.
[2] A.B. Stambouli, E. Traversa, Solid oxide fuel cells (SOFCs): a review of an environmentally clean and efficient source of energy, Renew. Sustain. Energy Rev. 6 (5) (2002) 433–455, https://doi.org/10.1016/S1364-0321(02)00014-X.
[3] N.Q. Minh, Solid oxide fuel cell technology—features and applications, Solid State Ionics 174 (1–4) (2004) 271–277, https://doi.org/10.1016/j.ssi.2004.07.042.
[4] A. Fernandes, T. Woudstra, A. van Wijk, L. Verhoef, P.V. Aravind, Fuel cell electric vehicle as a power plant and SOFC as a natural gas reformer: an exergy analysis of different system designs, Appl. Energy 173 (2016) 13–28, https://doi.org/10.1016/j.apenergy.2016.03.107.
[5] A. Choudhury, H. Chandra, A. Arora, Application of solid oxide fuel cell technology for power generation—a review, Renew. Sustain. Energy Rev. 20 (2013) 430–442, https://doi.org/10.1016/j.rser.2012.11.031.
[6] C. Bernay, M. Marchand, M. Cassir, Prospects of different fuel cell technologies for vehicle applications, J. Power Sources 108 (1–2) (2002) 139–152, https://doi.org/10.1016/S0378-7753(02)00029-0.
[7] S. Badwal, R. Deller, K. Foger, Y. Ramprakash, J. Zhang, Interaction between chromia forming alloy interconnects and air, Solid State Ionics 99 (1997) 297–310.
[8] L. Blum, W.A. Meulenberg, H. Nabielek, R. Steinberger-Wilckens, Worldwide SOFC technology overview and benchmark, Int. J. Appl. Ceram. Technol. 2 (6) (2005) 482–492.
[9] R.S. Gemmen, C.D. Johnson, Evaluation of fuel cell system efficiency and degradation at development and during commercialization, J. Power Sources 159 (1) (2006) 646–655, https://doi.org/10.1016/j.jpowsour.2005.10.109.
[10] H. Yokokawa, H. Tu, B. Iwanschitz, A. Mai, Fundamental mechanisms limiting solid oxide fuel cell durability, J. Power Sources 182 (2) (2008) 400–412, https://doi.org/10.1016/j.jpowsour.2008.02.016.
[11] C. Gindorf, Chromium vaporization from metallic interconnect and retention by perovskite layers, ECS Proceedings Volumes (1) (1999) 774–782, https://doi.org/10.1149/199919.0774PV, 1999-19.
[12] K. Hilpert, D. Das, M. Miller, D. Peck, R. Weiss, Chromium vapor species over solid oxide fuel cell interconnect materials and their potential for degradation processes, J. Electrochem. Soc. 143 (11) (1996) 3642.
[13] S. Heo, J. Hong, A. Aphale, B. Hu, P. Singh, Chromium poisoning of La 1-x Sr x MnO 3±δ cathodes and electrochemical validation of chromium getters in intermediate temperature-solid oxide fuel cells, J. Electrochem. Soc. 166 (13) (2019), https://doi.org/10.1149/2.0931913jes.
[14] S. Wang, T.A. Cruse, M. Krumpelt, B.J. Ingram, P.A. Salvador, Microstructural degradation of (La,Sr)MnO[sub 3]/YSZ cathodes in solid oxide fuel cells with uncoated E-Brite interconnects, J. Electrochem. Soc. 158 (2) (2011), https://doi.org/10.1149/1.3515073.
[15] E. Konysheva, et al., Chromium poisoning of perovskite cathodes by the ODS alloy Cr5Fe1Y2O3 and the high chromium ferritic steel Crofer22APU, J. Electrochem. Soc. 153 (4) (2006) A765–A773.
[16] S. Jiang, X. Chen, Chromium deposition and poisoning of cathodes of solid oxide fuel cells – a review, Int. J. Hydrogen Energy 39 (1) (2014) 505–531, https://doi.org/10.1016/j.ijhydene.2013.10.042.
[17] Z. Sun, S. Gopalan, U.B. Pal, S.N. Basu, Cu1. 3Mn1. 7O4 spinel coatings deposited by electrophoretic deposition on Crofer 22 APU substrates for solid oxide fuel cell applications, Surf. Coating. Technol. 323 (2017) 49–57.
[18] Z. Sun, R. Wang, A.Y. Nikiforov, S. Gopalan, U.B. Pal, S.N. Basu, CuMn1. 8O4 protective coatings on metallic interconnects for prevention of Cr-poisoning in solid oxide fuel cells, J. Power Sources 378 (2018) 125–133.
[19] K. Fujita, K. Ogasawara, Y. Matsuzaki, T. Sakurai, Prevention of SOFC cathode degradation in contact with Cr-containing alloy, J. Power Sources 131 (1–2) (2004) 261–269, https://doi.org/10.1016/j.jpowsour.2003.12.051.
[20] N. Shaigan, W. Qu, D.G. Ivey, W. Chen, A review of recent progress in coatings, surface modifications and alloy developments for solid oxide fuel cell ferritic stainless steel interconnects, J. Power Sources 195 (6) (2010) 1529–1542, https://doi.org/10.1016/j.jpowsour.2009.09.069.
[21] M. Stanislowski, et al., Reduction of chromium vaporization from SOFC interconnectors by highly effective coatings, J. Power Sources 164 (2) (2007) 578–589, https://doi.org/10.1016/j.jpowsour.2006.08.013.
[22] M. Krumpelt, et al., The effect of chromium oxyhydroxide on solid oxide fuel cells, J. Electrochem. Soc. 157 (2) (2010), https://doi.org/10.1149/1.3266930.
[23] S.C. Paulson, V.I. Birss, Chromium poisoning of LSM-YSZ SOFC cathodes, J. Electrochem. Soc. 151 (11) (2004), https://doi.org/10.1149/1.1806392.
[24] S. Taniguchi, et al., Degradation phenomena in the cathode of a solid oxide fuel cell with an alloy separator, J. Power Sources 55 (1) (1995) 73–79.
[25] R. Wang, U.B. Pal, S. Gopalan, S.N. Basu, Chromium poisoning effects on performance of (La,Sr)MnO 3 -based cathode in anode-supported solid oxide fuel cells, J. Electrochem. Soc. 164 (7) (2017), https://doi.org/10.1149/2.0441707jes.
[26] K. Yoon, P. Zink, S. Gopalan, U.B. Pal, Polarization measurements on single-step co-fired solid oxide fuel cells (SOFCs), J. Power Sources 172 (1) (2007) 39–49, https://doi.org/10.1016/j.jpowsour.2007.03.003.
[27] R. Wang, M. Würth, U.B. Pal, S. Gopalan, S.N. Basu, Roles of humidity and cathodic current in chromium poisoning of Sr-doped LaMnO3-based cathodes in solid oxide fuel cells, J. Power Sources 360 (2017) 87–97, https://doi.org/10.1016/j.jpowsour.2017.06.005.
[28] M.A. Laguna-Bercero, Recent advances in high temperature electrolysis using solid oxide fuel cells: a review, J. Power Sources 203 (2012) 4–16, https://doi.org/10.1016/j.jpowsour.2011.12.019.
[29] H. Kurokawa, C.P. Jacobson, L.C. DeJonghe, S.J. Visco, Chromium vaporization of bare and of coated iron–chromium alloys at 1073 K, Solid State Ionics 178 (3–4) (2007) 287–296, https://doi.org/10.1016/j.ssi.2006.12.010.
[30] Y. Matsuzaki, I. Yasuda, Electrochemical properties of a SOFC cathode in contact with a chromium-containing alloy separator, Solid State Ionics 132 (3–4) (2000) 271–278.
[31] S. Jiang, J. Zhang, L. Apateanu, K. Foger, Deposition of chromium species at Sr-doped LaMnO3 electrodes in solid oxide fuel cells. I. Mechanism and kinetics, J. Electrochem. Soc. 147 (11) (2000) 4013.
[32] M.C. Tucker, H. Kurokawa, C.P. Jacobson, L.C. Jonghe, S.J. Visco, A fundamental study of chromium deposition on solid oxide fuel cell cathode materials, J. Power Sources 160 (1) (2006) 130–138, https://doi.org/10.1016/j.jpowsour.2006.02.017.
[33] D. Röhrens, A. Neumann, A. Beez, I. Vinke, L. de Haart, N. Menzler, Formation of chromium containing impurities in (La, Sr) MnO3 solid-oxide-fuel-cell cathodes under stack operating conditions and its effect on performance, Ceram. Int. 42 (8) (2016) 9467–9474.
[34] X. Chen, L. Zhang, E. Liu, S. Jiang, A fundamental study of chromium deposition and poisoning at $(La_{0.8}Sr_{0.2})_{0.95}(Mn_{1-x}Co_x)O_{3\pm\delta}$ ($0.0 \leq x \leq 1.0$) cathodes of solid oxide fuel cells, Int. J. Hydrogen Energy 36 (1) (2011) 805–821, https://doi.org/10.1016/j.ijhydene.2010.09.087.